Design of DD Coil With High Misalignment Tolerance and Low EMF Emissions for Wireless Electric Vehicle Charging Systems

Kai Song, *Senior Member, IEEE*, Guang Yang, Yu Guo, Yu Lan, Shuai Dong, Jinhai Jiang, and Chunbo Zhu, *Member, IEEE*

***Abstract*—In this article, a design method of the double-D (DD) coil aiming at high misalignment tolerance is proposed, and the electromagnetic field (EMF) shielding of the system is considered. Inspired by the DD coil recommended in the standard J2954 published by the Society of Automotive Engineers, the novel structures of the transmitting (Tx) coil and the receiving (Rx) coil are designed, respectively. First, the standard DD coil is introduced as a reference. Second, for the Tx coil, the parameters, such as length, width, and coverage, are investigated in detail. For the Rx coil, the coil structure overlapped in the edge is optimized. The purpose is to obtain a higher coupling coefficient at the maximum offset. Third, considering EMF emissions exceeding the limit, the structure of the central-depressed coil with E-shaped cores is proposed in the Tx coil. The EMF emissions can be reduced to less than 27 μT at the rated output power. Finally, a 6.6–kW experimental system of which the maximum transmission efficiency is higher than 94% is set up. The experimental results prove that the proposed structure is beneficial to maintain a higher coupling coefficient against misalignment and suppress EMF emissions.**

***Index Terms*—DD coil, EMF emissions, misalignment tolerance, wireless electric vehicle charging.**

I. Introduction

WIRELESS charging is becoming popular since it does not need charging cables and is convenient to operate [1]–[3]. In recent years, a lot of wireless electric vehicle charging (WEVC) applications have been proposed, and the advantages, such as providing automatic charging, increasing device mobility, and reducing battery capacity, are highlighted [4]–[6]. In these applications, the circular coil and the square coil are widely used because of the simple structure and relatively low electromagnetic field (EMF) emissions [5]–[7]. However, the misalignment tolerance of these coils seems weak [8]. When the transmitting (Tx) coil and receiving (Rx) coil are not aligned, the coupling coefficient k always decreases significantly, which leads to low output power and transmission efficiency.

To improve k when the Tx coil and the Rx coil are misaligned, Budhia *et al*. [9] first proposed a new polarized coil structure as a double D (DD). Compared with the square coil, the DD coil can provide a charge zone five times larger for a similar material cost [9]. Another advantage is that k remains constant within a certain lateral offset of the Rx coil. It is beneficial to WEVC systems because the parking locations are usually not fixed and the misalignment tolerance is crucial [10], [11]. The standard J2954 published by the Society of Automotive Engineers (SAE) also recommended DD coils for different power levels, which proves that the DD coil is widely used in industry [12].

In this article, two research hotspots of the DD coil are selected for investigation. First, although SAE J2954 has specified some important coil parameters, it is uncertain whether these parameters reach the optimal values. For example, as the DD coil is designed to improve the misalignment tolerance of traditional unipolar coils, whether the misalignment tolerance can be further enhanced becomes a problem worthy of study. Budhia *et al*. [9] summarized some design parameters of the DD coil to improve k, which motivates the study of this article. A novel DD coil with a quadrature coil, which is called DDQ pad, was also proposed in [9]. The misalignment tolerance of the lateral and horizontal directions can be improved simultaneously. But two sets of independent rectifier with filter are needed, which makes the vehicle-side complex. Li *et al*. [13] also adopted the method of coil combination and proposed a solenoid DD (SDD) coil. A good tolerance for air gap variation and horizontal misalignment was validated. The coil combination is useful, but adding coils will cause additional losses and complexity. Li *et al.* [14] proposed a novel Taichi coil and proved that it could improve the lateral misalignment tolerance compared with the DD coil. Generally, some methods have been proposed to improve the misalignment tolerance of the DD coil. However, these methods are at the cost of increasing the structural complexity of the DD coil.

Second, the safety problems caused by the EMF leakage in practical applications need to be considered. EMF emissions are not only serious health concerns but also may interfere

Manuscript received October 23, 2019; revised January 7, 2020; accepted February 1, 2020. Date of publication February 6, 2020; date of current version May 1, 2020. This work was supported in part by the National Natural Science Foundation of China under Grants 51677032 and 51977043, in part by the Natural Science Foundation of Heilongjiang Province under Grant E2017045, and in part by the Harbin Science and Technology Innovation Talents Special Fund Project under Grant 2016RAQXJ002. Recommended for publication by Associate Editor M. Ponce-Silva. *(Corresponding author: Shuai Dong.)*

Kai Song, Guang Yang, Yu Lan, Shuai Dong, Jinhai Jiang, and Chunbo Zhu are with the School of Electrical Engineering & Automation, Harbin Institute of Technology, Harbin 150001, China (e-mail: kaisong@hit.edu.cn; wesleyyang0721@163.com; 2104505717@qq.com; dongshuai@hit.edu.cn; 327616294@qq.com; zhuchunbo@hit.edu.cn).

Yu Guo is with Shenzhen Inovance Technology Company, Ltd., Shenzhen 518000, China (e-mail: guoyu079@163.com).

Color versions of one or more of the figures in this article are available online at https://ieeexplore.ieee.org.

Digital Object Identifier 10.1109/TPEL.2020.2971967

with other vehicle-side electronic systems, such as remote start systems [15]. The most popular EMF shielding method is to place aluminum (Al) plates under the Tx coil and above the Rx coil, respectively, [16]. Lin *et al*. [17] proposed an optimized core structure that can realize better shielding for the DD coil. By extending the core past the ends of the coils in each pad, the flux generated by the Tx coil will be attracted and not be coupled to the Rx coil or leak. Furthermore, Mohammad *et al*. [16] analyzed the EMF emission limit recommended by the International Commission of Non-Ionized Radiation Protection (ICNIRP). Then, a shielding method using a combination of Al shielding and magnetic shielding is proposed. This method is far more effective than Al shielding. However, additional cores will increase the weight and volume of the magnetic coupler, which is not expected for the miniaturization of vehicle-side equipment.

From the abovementioned discussion, existing research works on misalignment tolerance improvement and EMF suppressing for the DD coil can be supplemented.

1) Previous studies have focused on changing the structure of DD coils, such as designing DDQ pad or SDD coils, to improve the misalignment tolerance. However, if we do not want to alter the DD coil to other coil structures, the coil parameters need to be reoptimized, and the general method needs to be concluded.
2) After the coil parameters are redesigned, it is questionable whether the original Al shielding is effective. Thus, the effectiveness of Al shielding under different coil parameters needs to be analyzed. If it fails to reduce the leakage, the other EMF shielding methods are worth studying. For instance, the ferrite shielding proposed in [16] is useful, especially for the case with misalignment. However, it may lead to additional core consumption and an increase in weight. The tradeoff between effectiveness, complexity, and material consumption needs further investigation.

Considering the issues of current research works, the purpose of this article is to propose a design method of the DD coil to obtain better misalignment tolerance and lower EMF emissions. Some information needs to be declared as follows.

1) For health reasons, the ICNIRP guideline provides that the root-mean-square (rms) value of the exposed flux density for 3–100 kHz cannot exceed 27 μT. Thus, 27 μT is selected as a reference value for finite-element analysis (FEA) simulation in this article.
2) Since EMF emissions are related to system power level [14], to comply with SAE J2954, this article selects a WPT2 (the output power is 6.6 kW)/Z2 (the transmission distance varies from 140 to 210 mm) charger to validate the research.

The remaining of this article is structured as follows. In Section II, the DD coil recommended in SAE J2954 is introduced. Aiming at improving the coupling coefficient against misalignment, the Tx coil and Rx coil are designed in Section III. Then, in Section IV, the central-depressed coil with E-shaped cores is proposed in the Tx coil. The experimental results are provided in Section V. Finally, Section VI concludes this article.

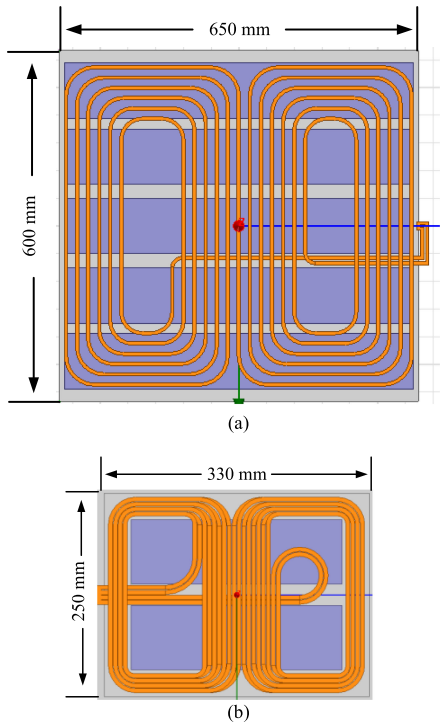

Fig. 1. Standard coils in SAE J2954 (WPT2/Z2) [12]. (a) Tx coil. (b) Rx coil.

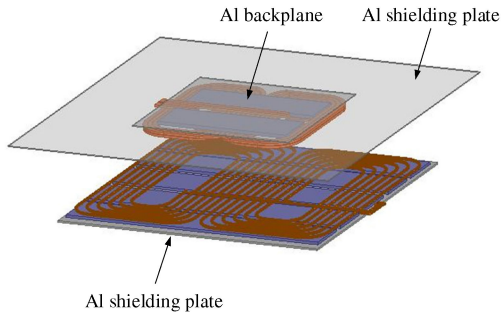

Fig. 2. Al shielding in SAE J2954.

II. DD Coil in SAE J2954

A. Parameters of the Coil

Taking WPT2/Z2 as an example, the standard coil is shown in Fig. 1 [12]. The size of the Tx coil is about 650 × 600 mm, and that of the Rx coil is 330 × 250 mm. For the Tx coil, the larger size is designed to cover different air gaps. Also, the asymmetric structure guarantees the stability of transmission efficiency when the coils are misaligned [18]. Smaller Rx coil is chosen to reduce the weight of vehicle-side equipment. Cores and Al plates are located below the Tx coil and upper the Rx coil, respectively, to enhance coupling and realize EMF shielding.

B. Al Shielding and Shielding Effectiveness

Al shielding is recommended in SAE J2954, as shown in Fig. 2. For low-frequency magnetic field, it is easy to use cores to shape the flux and avoid leakage because of its high permeability [4]. However, cores are not suitable for high-frequency magnetic

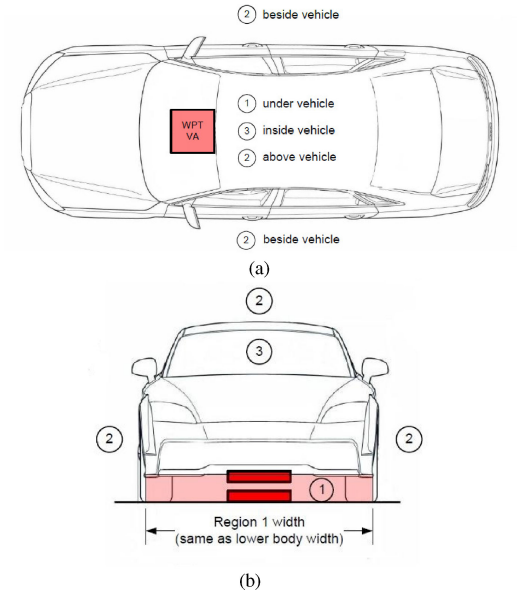

Fig. 3. Defined EMF regions in SAE J2954 [12]. (a) Top view. (b) Front view.

field shielding because the high hysteresis loss leads to the decline of system quality factor [19]. Thus, Al plates with high conductivity are applied. Due to the eddy current effect, the generated reverse magnetic field can weaken the flux leakage [20].

Mohammad *et al.* [16] introduced shielding effectiveness (SE) to evaluate the shielding method. The SE is defined as follows:

$$SE = 20 \lg \frac{H_0}{H_1} \tag{1}$$

where H_0 and H_1 are the rms values of the magnetic field strength measured at the same test point without and with shielding, respectively. The more effective a shielding method, the lower H_1 is, and the corresponding SE will increase. Thus, SE can be introduced to evaluate how effective the shielding method is. In this article, the SE of several methods is compared at different test points to prove the proposed method can realize better shielding.

C. EMF Emission Limit and Test Points

As illustrated above, for an 85-kHz charging system, the flux density cannot exceed the ICNIRP threshold of 27 $\mu\mathrm{T_{RMS}}$ at all test points. Three regions are defined to facilitate EMF safety management in SAE J2954, as shown in Fig. 3. Region 2 and Region 3 are exposed to drivers and pedestrians. Therefore, in this article, three measurement lines are set in Region 2 and Region 3, respectively, as shown in Fig. 4. Only the flux density along each line is less than 27 $\mu\mathrm{T_{RMS}}$ can the shielding be validated.

III. Research on Misalignment Tolerance Improvement

The diagram of a typical WEVC system is shown in Fig. 5. When the DD coil is applied, the output characteristics, such as output power and coil to coil efficiency, can be obtained [11],

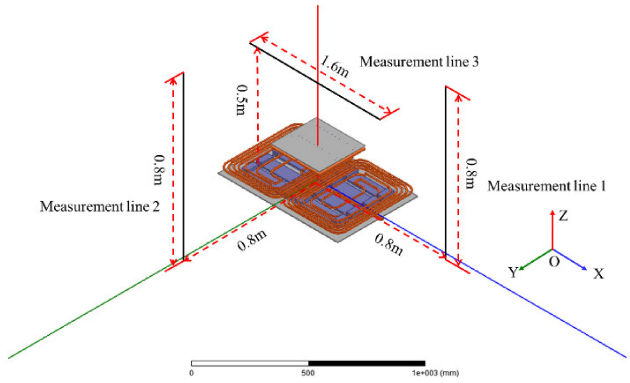

Fig. 4. Measurement lines designed in this article.

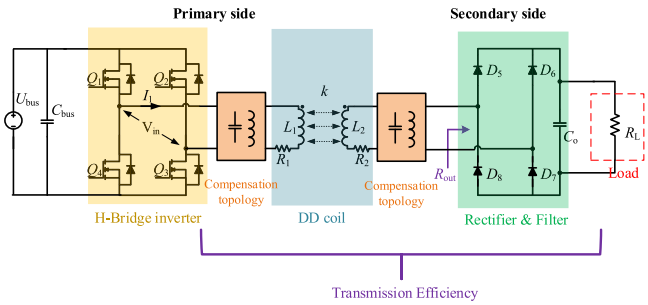

Fig. 5. Typical WEVC system diagram.

[21]. The output power P_{out} is calculated as follows:

$$P_{\mathrm{out}} = P_{\mathrm{su}} Q_2 = V_{\mathrm{in}} I_1 k^2 Q_2 \tag{2}$$

$$Q_2 = \frac{\omega L_2}{R_{\mathrm{out}}} \tag{3}$$

where P_{su} is the uncompensated power and can be used to evaluate system power capacity. Q_2 is the quality factor of the receiver circuit, and it is always limited to 4–6 in practical applications [11]. Also, it is easy to obtain the maximum coil to coil efficiency as follows:

$$\eta_{\max} = \frac{k^2 Q_p Q_s}{\left(1 + \sqrt{1 + k^2 Q_p Q_s}\right)^2} \tag{4}$$

$$Q_p = \frac{\omega L_1}{R_1} \tag{5}$$

$$Q_s = \frac{\omega L_2}{R_2} \tag{6}$$

where Q_p and Q_s are the quality factors of the Tx and the Rx coil, respectively [21]. Their values are usually stable, reaching several hundred in WEVC systems.

To realize the maximum efficiency, Yang *et al.* [4] demonstrated that the optimal load is essential. Only if the load is matched to the optimal one, the maximum efficiency can be achieved. The optimal load can be derived as

$$R_{\mathrm{opt}} = \sqrt{\frac{R_2}{R_1}(R_1 R_2 + \omega^2 k^2 L_1 L_2)}. \tag{7}$$

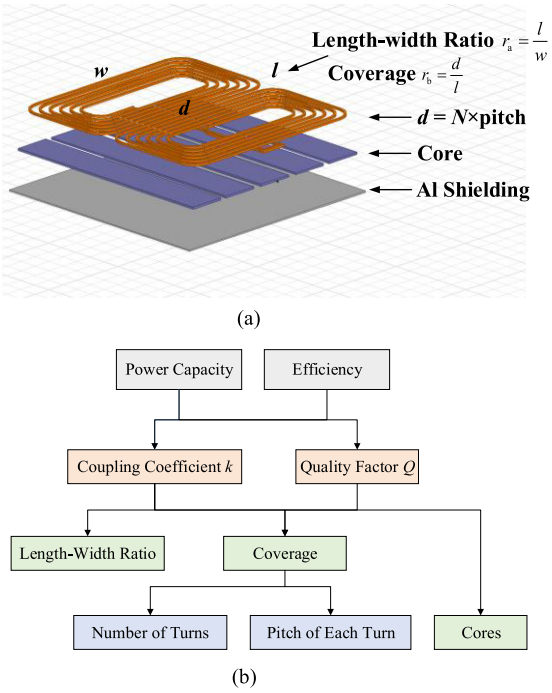

Fig. 6. Design parameter of the DD coil. (a) Parameters in three-dimensional view. (b) Relationship of the parameters.

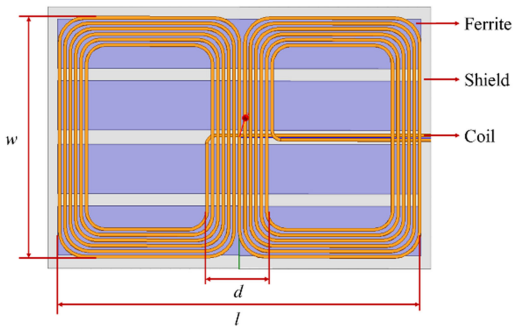

Fig. 7. Length–width ratio and coverage.

Equations (2) and (4) show that the optimization of the DD coil can be carried out from k and Q. Since Q is relatively stable, k is easier to be improved by comparison. Two important parameters, length–width ratio r_a and coverage r_b, are chosen to be designed for higher k in this article, as shown in Fig. 6. Additionally, the inverter is not the focus of this article, so the efficiency from inverter output to load is defined as the transmission efficiency and discussed in the following sections.

A. Length–Width Ratio

As shown in Fig. 7, the length–width ratio r_a can be expressed as

$$r_a = \frac{l}{w}. \tag{8}$$

Assuming that all the simulated coil models have the same product of length and width, by FEA simulation, the trend of k versus offset under different r_a is shown in Fig. 8. For X offset, k keeps relatively high when r_a is 1.5 or 1.6. Meanwhile, under r_a of 1.6, the stability of k is improved slightly. For Y offset, k is almost the same when r_a varies from 1.3 to 1.6. It is also noted that k decreases obviously, and its stability against offset declines if r_a exceeds 1.7. Thus, taking the tradeoff of misalignment tolerance and practical installation, this article designs r_a as 1.5.

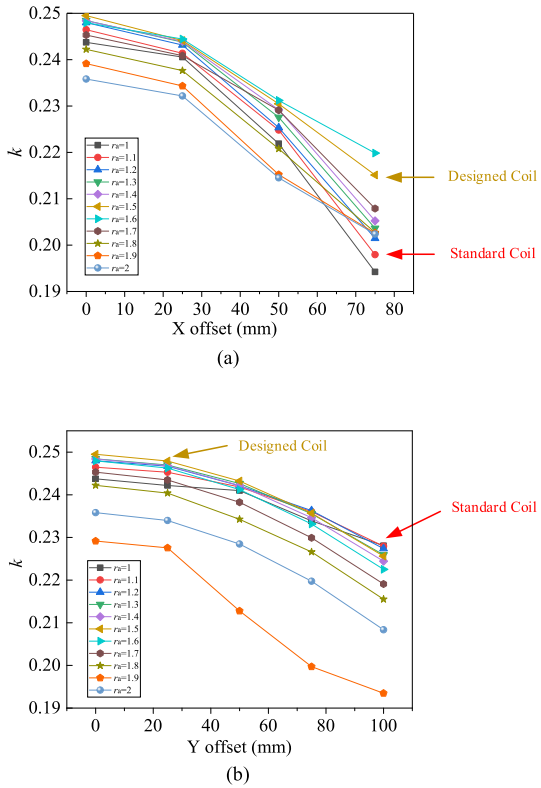

Fig. 8. k versus offset under different r_a. (a) X offset. (b) Y offset.

B. Coverage

The coverage r_b is a parameter that distinguishes the DD coil from the circular coil, and it is defined as

$$r_b = \frac{d}{l} \tag{9}$$

r_b is mainly determined by the number of turns N and pitch of each turn [11]. Therefore, the two aspects are studied in this article. First, the coil is close winding (pitch ≈ 0) when studying the effect of N. As shown in Fig. 9, k is almost independent of N, whereas P_{su} increases with the growth of N. Combined with (2), it is clear that P_{out} is desirable during N varying from 4 to 9.

Second, the effect of the pitch is investigated. Fig. 10 presents the coil models with the same N and different pitches. It can be seen that r_b increases if the pitch gets large. Based on these models, the trend of k versus r_b under different N is depicted in Fig. 11. r_b of 10% represents close winding. From Fig. 11, the following conclusions can be summarized.

1) If N is fixed, k increases first and then decreases with r_b. When the coils are aligned and the air gap is minimum,

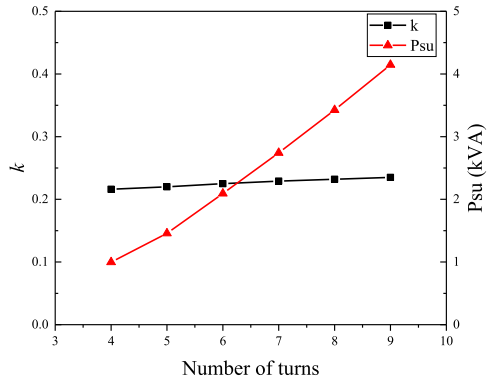

Fig. 9. Influence of N on k and P_{su}.

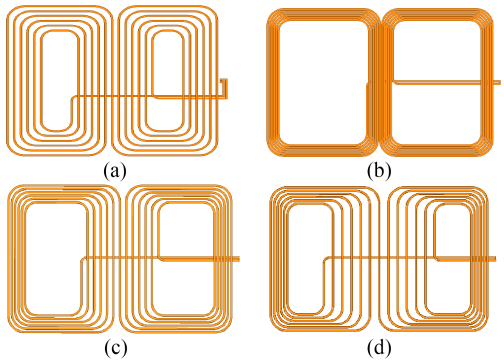

Fig. 10. Coil models with different r_b. (a) $r_b = 40\%$ (SAE coil). (b) $r_b = 10\%$. (c) $r_b = 35\%$. (d) $r_b = 45\%$.

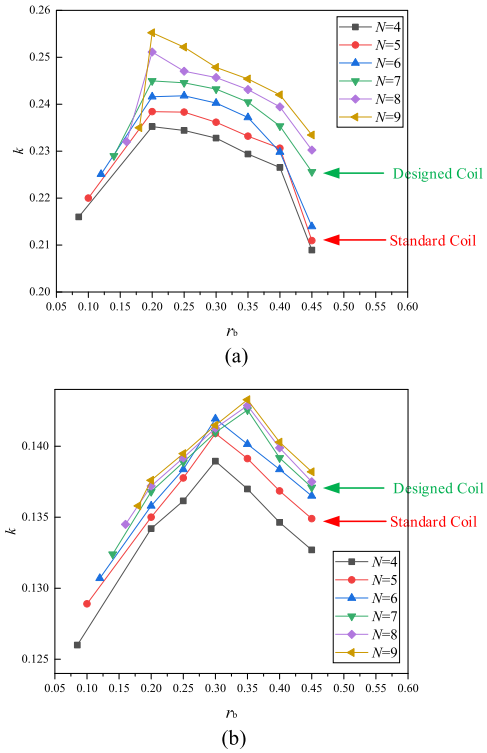

Fig. 11. k versus r_b under different N. (a) No offset. (b) Maximum offset.

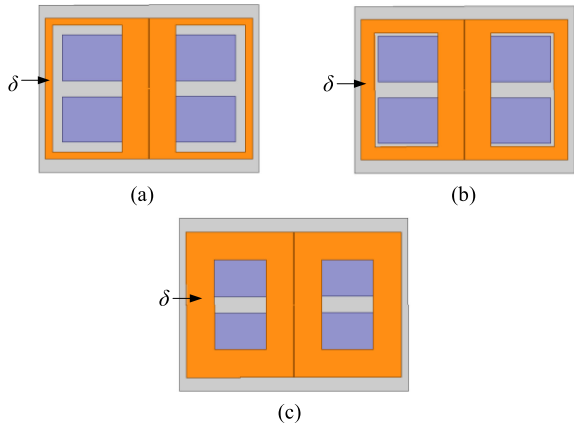

Fig. 12. Coil models with different δ. (a) $\delta = 10$ mm. (b) $\delta = 20$ mm. (c) $\delta = 40$ mm.

the maximum k occurs at r_b of 20%–25%. However, with the maximum offset, r_b should be 30%–35%.

2) If N is not fixed, generally, k of the same r_b has little difference. N and r_b have little effect on k when the coils are aligned and the air gap is minimum. Therefore, k with the maximum offset attracts more attention. Considering both high misalignment tolerance and Litz wire consumption, N is set as 7, and r_b is designed to be 35% in this article.

C. Design of Rx Coil

As recommended in SAE J2954, the Rx coil is characterized by the overlapping in edge. In this section, the influence of the overlapping is analyzed. We established Rx coil models with different overlapping, as shown in Fig. 12.

δ is used to represent the numbers of the overlapped layers. The smaller δ is, the more layers are overlapped. δ is 40 mm, 20 mm, and 10 mm, which represent no layers, two layers, and three layers are overlapped, respectively. The trend of k is plotted in Fig. 13. We can find that k increases after the layers are overlapped. As more and more layers are overlapped, k will not change a lot, but the coil is getting thicker. Taking the tradeoff of k and the coil thickness, a two-layer overlapping is adopted, as shown in Fig. 14.

D. Comparison With Standard Coil

k of the designed coil and the standard one are simulated, respectively, and compared. The results are plotted in Fig. 15. k of the designed coil is higher than that of the standard coil when the offset increases, which is beneficial to improving the misalignment tolerance.

IV. Optimized Structure for EMF Shielding

A. Analysis of Core Length

The simulated flux distribution of the DD coil is shown in Fig. 16. Φ_M is the main flux that contributes to magnetic coupling. Φ_1, Φ_2, Φ_4, and Φ_5 are the possible flux leakages without shielding.

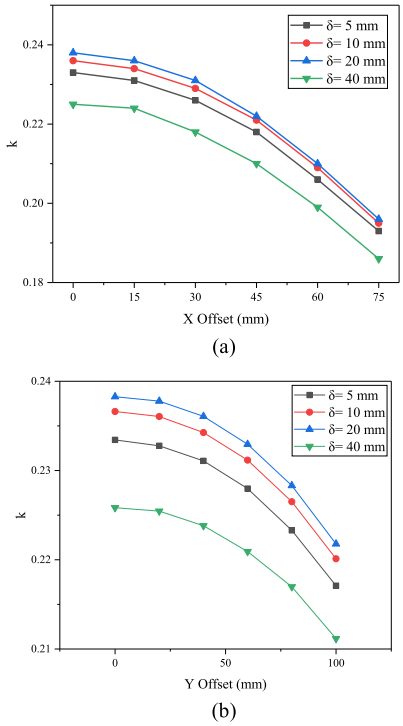

Fig. 13. Comparison of k under different δ. (a) k versus X offset. (b) k versus Y offset.

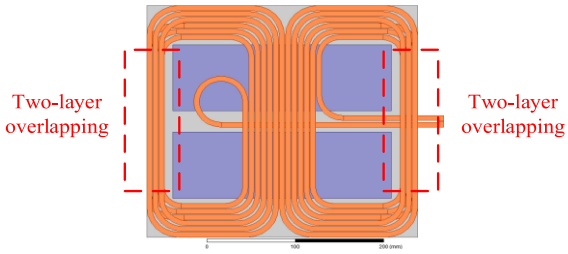

Fig. 14. Two-layer overlapped Rx coil.

The magnetic circuit model is established in Fig. 17. F_1 and F_2 represent the magnetic motive forces generated by the DD coil. R_{air} and R_{core} imply the magnetic reluctances of each magnetic circuit. The flux leakages Φ_1, Φ_2, Φ_4, and Φ_5 can be calculated as follows:

$$\Phi_1 = \frac{F_1}{R_{air-1} + R_{\text{core}-1}} \quad \Phi_2 = \frac{F_2}{R_{\text{air}-2} + R_{\text{core}-3}} \tag{10}$$

$$\Phi_4 = \frac{F_1 + F_2}{R_{\text{air}-4} + R_{\text{core}-2}} \quad \Phi_5 = \frac{F_1 + F_2}{R_{\text{air}-5} + R_{\text{core}-4}}. \tag{11}$$

F_1 and F_2 are determined by power levels and supposed to be constant. From (11), Φ_1 and Φ_2 can be suppressed by increasing $R_{\text{core-1}}$ and $R_{\text{core-3}}$. In general, the magnetic reluctance R_{core} is expressed as follows:

$$R_{\text{core}} = \frac{l}{\mu A} \tag{12}$$

where l means the core length, μ is the permeability, and A represents the effective area of the core. Thus, the core length

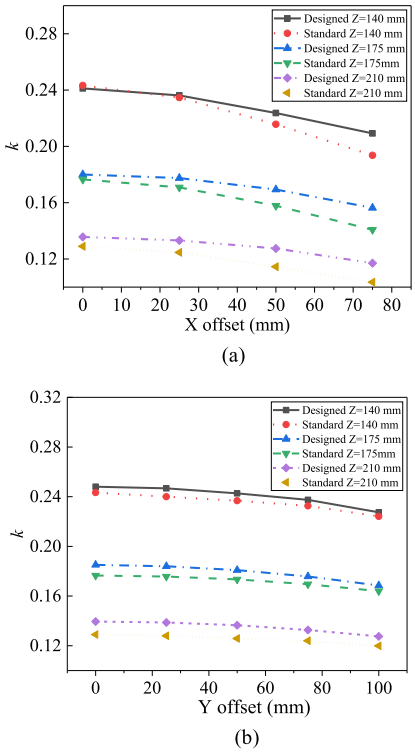

Fig. 15. Designed coil versus standard coil (without central-depressed structure). (a) X offset. (b) Y offset.

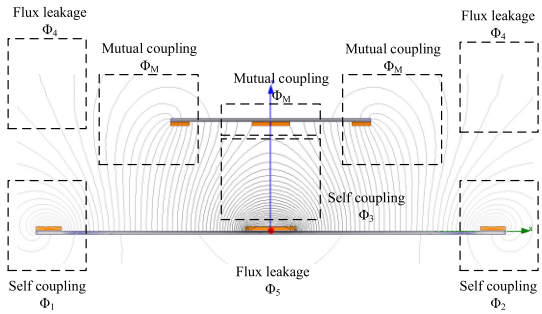

Fig. 16. Simulated flux distribution.

should be increased. Equation (11) also proves that the increase in the core length is beneficial to reduce the impact of Φ_4 and Φ_5. In this article, the length of the strip cores is extended to be the same as the length of the coil, as shown in Fig. 18.

The flux density distributions before and after increasing the core length are shown in Fig. 19. It can be seen that the flux leakage around the vehicle is significantly suppressed. However, the flux density above the Rx coil still exceeds the limit.

Table I lists the calculated maximum SE at different measurement lines shown in Fig. 5. From Table I, the following can be concluded.

1) SE will decline with misalignment. Thus, misalignment is harmful to EMF shielding.
2) The values of SE in Table I are relatively low, which means the method of increasing the core length is insufficient and can be improved.

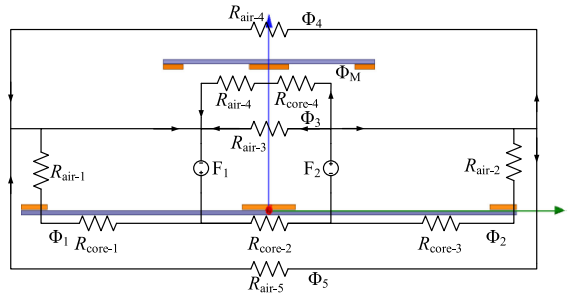

Fig. 17. Magnetic circuit model.

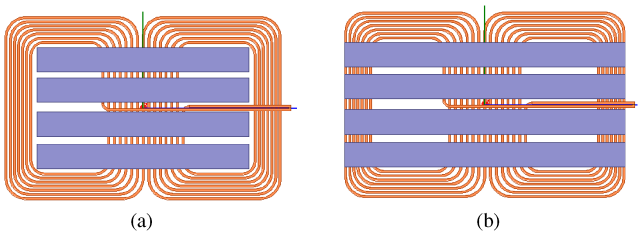

Fig. 18. Different core lengths. (a) Short core. (b) Long core.

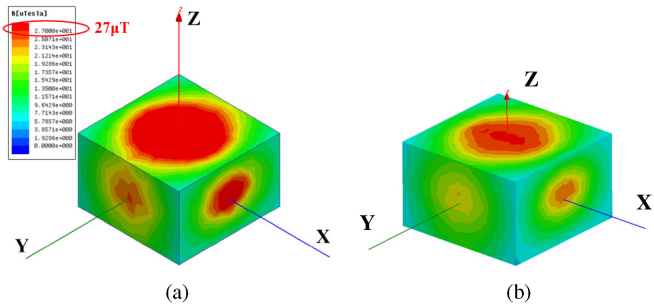

Fig. 19. Flux leakage of two kinds of core structures. (a) Short core. (b) Long core.

TABLE I
MAXIMUM SE AT DIFFERENT MEASUREMENT LINES

	Measurement Line 1	Measurement Line 2	Measurement Line 3
No Offset	3.12 dB	2.24 dB	3.01 dB
Maximum Offset	2.11 dB	2.20 dB	2.51 dB

3) The SE at measurement line 1 decreases more than the one at measurement line 2 because the DD coil has better misalignment tolerance in the *Y*-direction. When the Rx coil moves, the flux distribution will not be influenced significantly. Therefore, for the DD coil, measurement line 2 is relatively not critical in the three lines.

B. Optimization of Pitch of Each Turn

In Section III, the pitch of each turn is optimized for higher *k*. Keeping the coverage and the number of turns fixed, the pitch is adjusted, as shown in Fig. 20.

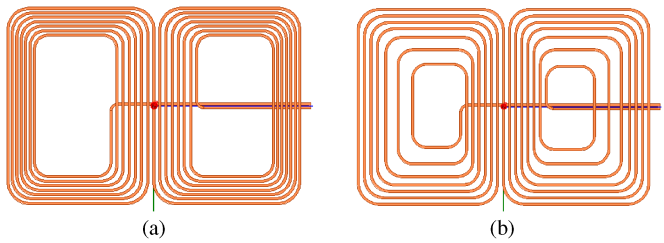

Fig. 20. Optimization of pitch. (a) Before adjustment. (b) After adjustment.

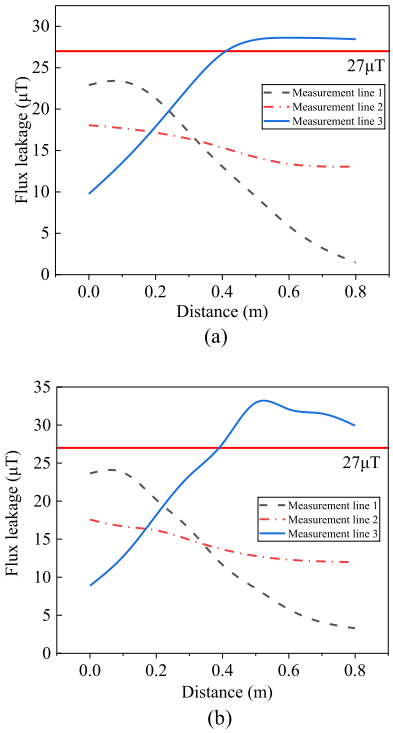

Fig. 21. Flux leakage after pitch optimization. (a) No offset. (b) Maximum offset.

After the pitch is optimized, the flux density along each measurement line is plotted in Fig. 21. This method can reduce the flux leakage on the side of the vehicle, but fail to suppress the flux leakage above the vehicle.

C. Central-Depressed Coil With E-Shaped Cores

As illustrated above, the abovementioned two methods fail to make the flux leakage lower than the limit. Therefore, the two approaches are combined, and the coil structure is redesigned, as shown in Fig. 22.

Compared with the conventional one, the part marked by the dotted frame is designed to move down by about 10 mm. Also, combined with (10) and (12), a small number of cores are added to convert strip cores into E shape so that the core length can be further increased, as shown in Fig. 23. To accommodate the thickness of the added cores, 10 mm is selected

When the proposed structure is applied, the flux density distribution is simulated, as shown in Fig. 24. Compared with the two methods mentioned before, the flux density is lower than 27

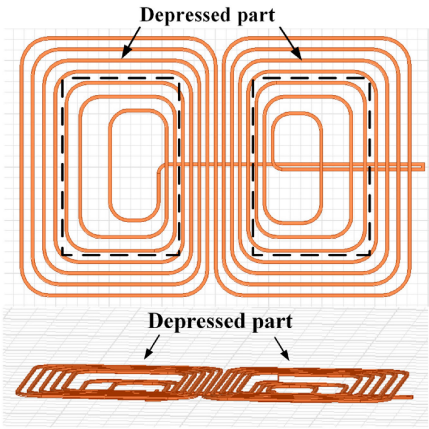

Fig. 22. Proposed central-depressed coil.

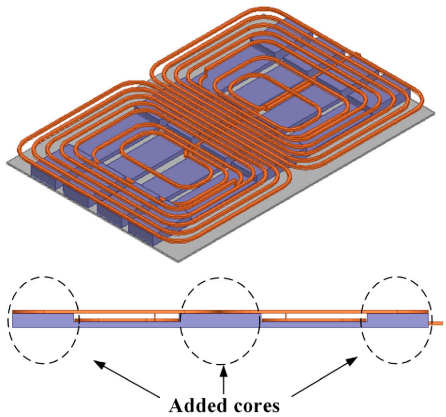

Fig. 23. Central-depressed coil with E-shaped cores.

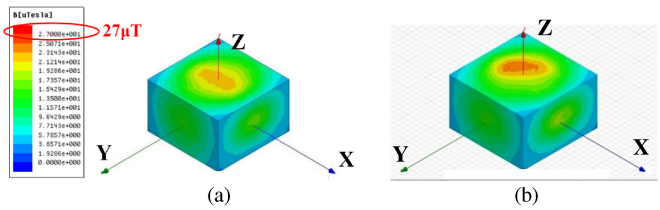

Fig. 24. Flux leakage of the proposed structure. (a) No offset. (b) Maximum offset.

μT_{RMS} even under the maximum offset. The simulation results of the flux density along measurement lines also prove the same conclusion, as shown in Fig. 25.

To further verify that the proposed method is reliable, with the maximum offset, the values of SE of the three methods are calculated and listed in Table II. It is easy to observe that the proposed structure can achieve the highest SE at each measurement line, which means that the central-depressed coil with E-shaped cores is the most effective in EMF shielding.

When the central-depressed coil with E-shaped cores is applied, the variation of k is analyzed. The simulation results of k are shown in Fig. 26. Compared with Fig. 15, although the proposed structure leads to the decrease in k, it is still

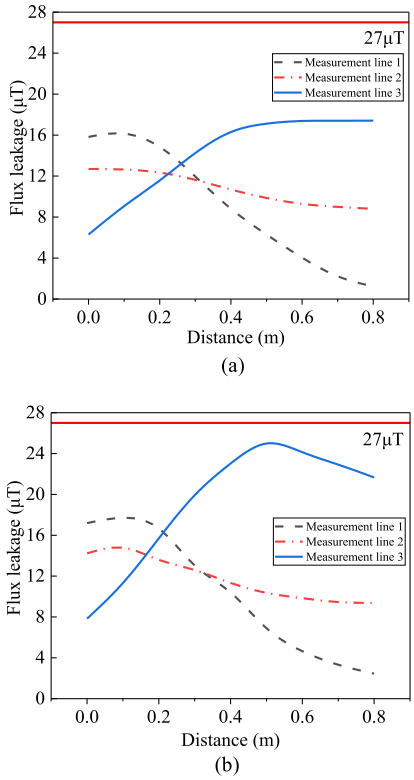

Fig. 25. Flux density along each measurement line. (a) No offset. (b) Maximum offset.

TABLE II
COMPARISON OF MAXIMUM SE OF THREE METHODS

Methods	Measurement Line 1	Measurement Line 2	Measurement Line 3
Increase Core Length	2.11 dB	2.20 dB	2.51 dB
Increase Pitch	4.26 dB	4.18 dB	4.11 dB
Proposed Structure	6.23 dB	5.77 dB	6.18 dB

obviously higher than the standard value, especially when X offset increases. Thus, it can be concluded that the proposed structure can achieve better misalignment tolerance and EMF shielding.

V. EXPERIMENTAL VALIDATION

A. Experimental Setup

An experimental system shown in Fig. 27(a) is built to validate the proposed design method. The system consists of an inverter, compensation capacitors, magnetic coupler, rectifier with capacitive filter, and load. An 800 × 800 mm Al shielding plate will be put above the Rx coil, as shown in Fig. 27(b). To simulate the possible misalignment between coils, a moveable bench is designed. The Rx coil can move along the *X*-/*Y*-/*Z*-axis. The waveforms are recorded by the oscilloscope Tektronix MDO3054, and the transmission efficiency is measured by the power analyzer

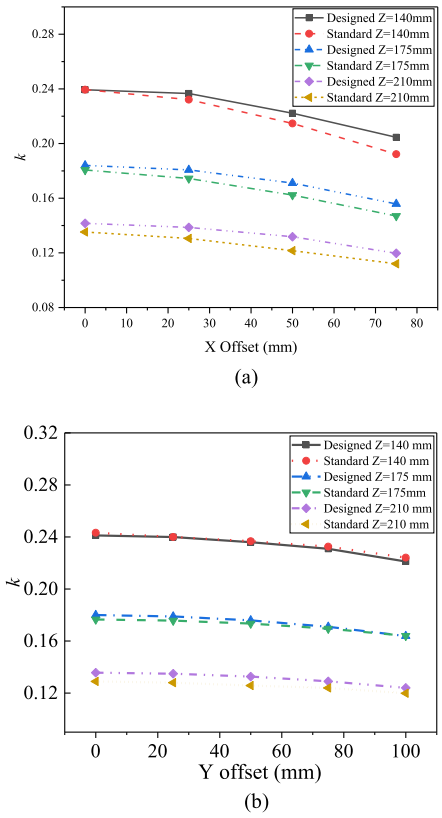

Fig. 26. Designed coil versus standard coil (with central-depressed structure). (a) *X* offset. (b) *Y* offset.

TABLE III
PARAMETERS OF DESIGNED DD COILS

Parameters	Tx Coil	Rx Coil
Dimension (Length × Width)/mm	750 × 500	320 × 250
Number of Turns	7	6
Litz Wire Diameter/mm	6	5
Self-Inductance/μH	63.1	40.5
Internal Resistance/mΩ	85	70
Coupling Coefficient	0.12~0.24	

Yokogawa PX8000. Field strength meter NARDA EHP-200 is utilized to record the flux density.

The designed coils are shown in Fig. 28. The detailed parameters are listed in Table III.

B. Experiments on Output Characteristics

In this section, output power, transmission efficiency, and misalignment tolerance are measured. First, the optimal load corresponding to the maximum efficiency is calculated as (7). A resistor of 6.8 Ω is selected. It is found that the output power meets WPT2 requirements and the maximum transmission efficiency can realize 95%, as shown in Fig. 29. The waveforms of

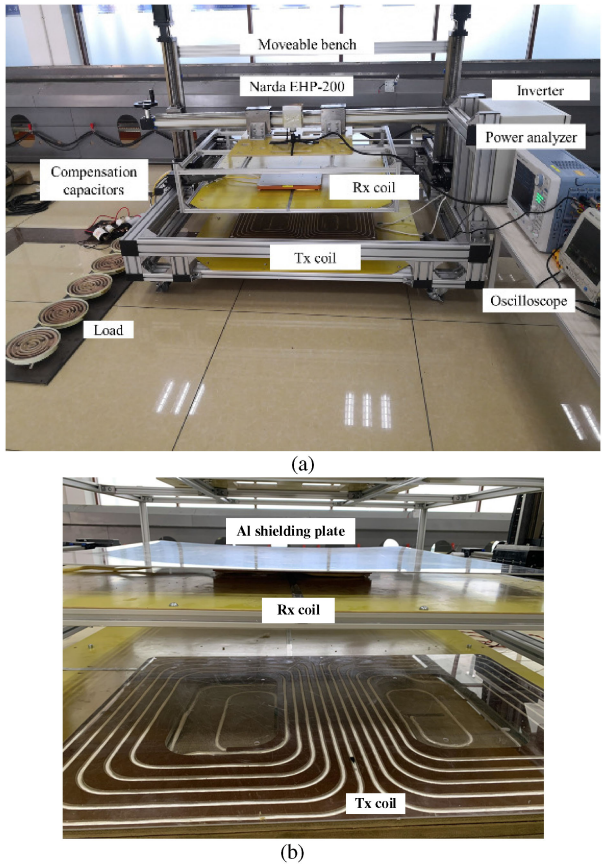

Fig. 27. Experimental system. (a) Overall view. (b) Adding a Al shielding.

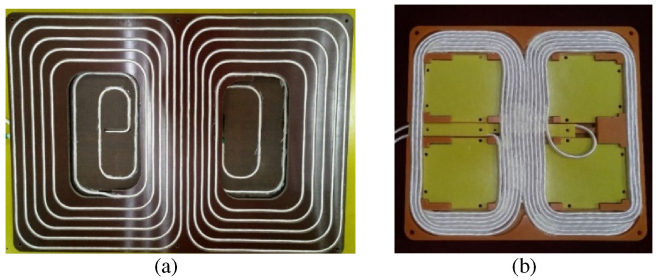

Fig. 28. Designed DD coil. (a) Tx coil. (b) Rx coil.

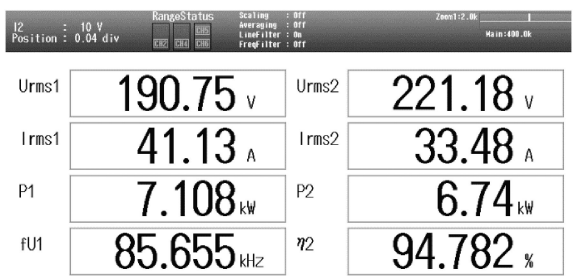

Fig. 29. Output power and transmission efficiency (using the optimal load).

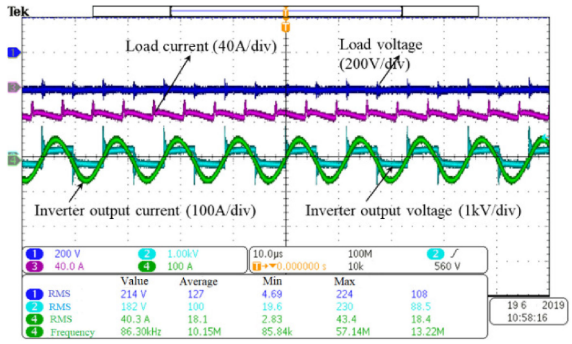

Fig. 30. Inverter output voltage/current and load voltage/current.

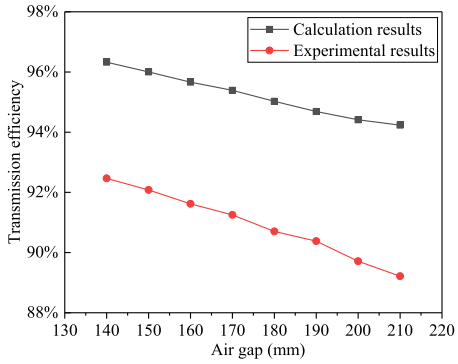

Fig. 31. Transmission efficiency versus air gap.

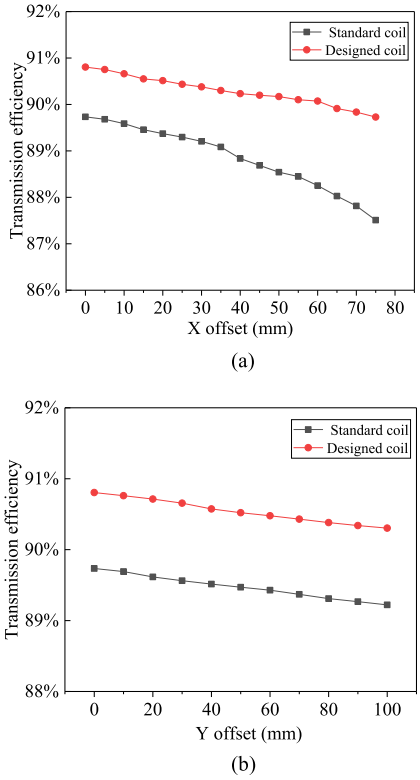

Fig. 32. Transmission efficiency versus offset ($Z = 175$ mm). (a) X offset. (b) Y offset.

the inverter output voltage/current and the load voltage/current are shown in Fig. 30. The inverter output voltage and current are in phase, which implies that the reactive power is almost eliminated.

Second, to simulate the voltage range of the real batteries (250–420 V), the load resistance is changed to 10 Ω. The influence of the air gap and offset are investigated. When the air gap varies from 140 to 210 mm, the transmission efficiency is recorded and plotted in Fig. 31. The calculated value is obtained by (2). From Fig. 31, it is found that the transmission efficiency declines with the increased air gap. The difference between the calculated value and the measured one may be caused by the internal resistance of the capacitor and the core loss.

Third, the transmission efficiency is measured when the coils are misaligned. Since this article concentrates on the coupling coefficient improvement for the misaligned coils, Fig. 32 depicts the trend of the transmission efficiency versus offset. X offset has a great influence on efficiency, whereas the efficiency remains stable against Y offset. Compared with the standard coil, the transmission efficiency of the optimized coil is higher, no matter in which direction the offset occurs. The abovementioned results prove the misalignment tolerance is improved after optimization.

Through the abovementioned experiments, it can be concluded that after optimizing the structure of the DD coil, the transmission efficiency and misalignment tolerance are improved simultaneously compared with the standard coil. EMF shielding performance will be verified below.

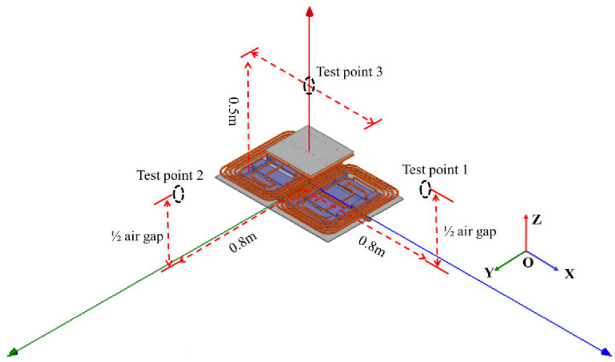

Fig. 33. Test points in the experiments.

C. Validation of the Proposed Shielding Method

As illustrated in Section II-C, flux leakage in the defined regions needs to meet the ICNIRP guideline. A series of test points are chosen, as shown in Fig. 33.

At these test points, the flux density in the frequency band from 60 to 100 kHz is obtained, as shown in Figs. 34 and 35, respectively. Fig. 33 shows the flux density when the coils are aligned and the air gap is the minimum. Since Narda EHP-200 consists of three magnetic induction coils placed orthogonal to each other, the pink, green, and blue curve imply the X, Y, and Z components of the exposed flux density we want to measure, respectively. The rms value of the total flux density is calculated and shown by the purple curve. The maximum value

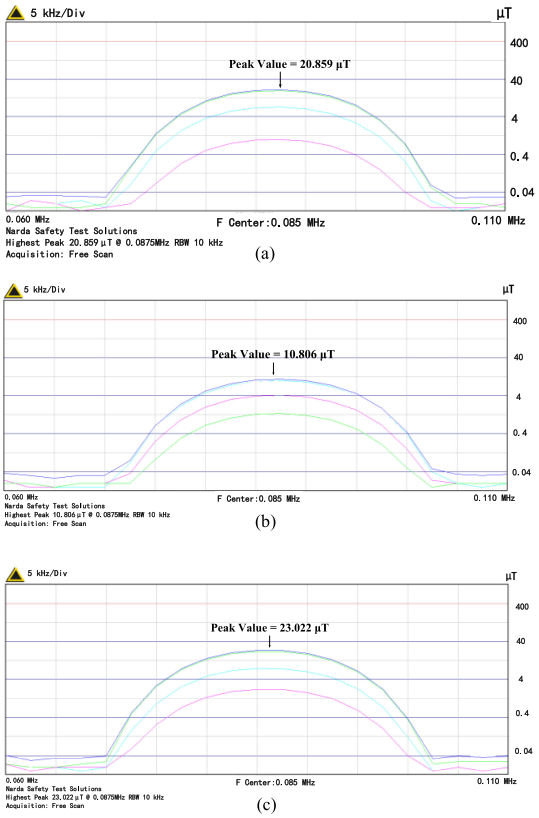

Fig. 34. Flux density at the test points (no offset). (a) Test point 1. (b) Test point 2. (c) Test point 3.

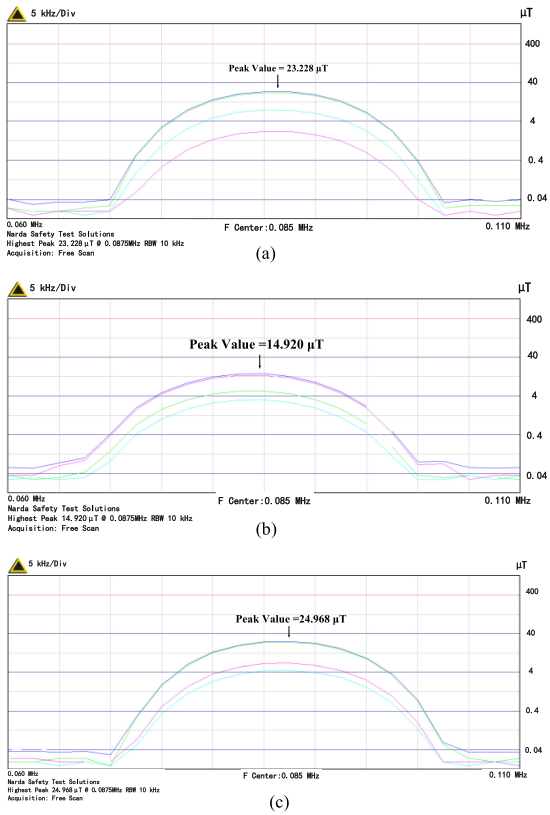

Fig. 35. Flux density at the test points (maximum offset). (a) Test point 1. (b) Test point 2. (c) Test point 3.

of 23.022 μT appears at test point 3, which implies that the system satisfies the ICNIRP guideline.

With the maximum offset, Fig. 35 implies that the exposed flux density is higher, and the maximum value increases to about 25 μT. Refer to the ICNIRP guideline, the security of the system is still guaranteed.

In conclusion, the DD coil designed in this article has two characteristics.

1) Within the same offset range, the decline of the coupling coefficient is slower. The trend of the transmission efficiency is consistent, which means that the misalignment tolerance of the designed coil is improved.
2) The exposed flux density at all test points is less than 27 $\mu\mathrm{T}_{\mathrm{RMS}}$, which means the system is safe.

VI. Conclusion

This article proposes a design method of the DD coil for high misalignment tolerance and effective EMF shielding. Referring to the WPT2/Z2 DD coil recommended in SAE J2954, the coil parameters, including the length–width ratio, the coverage, and the overlapping are redesigned. The design makes the decline of the coupling coefficient against the offset slower. However, it is found that the EMF emissions exceed the limit. Therefore, the middle part of the Tx coil is designed to be depressed, and the E-shaped cores are applied. The proposed structure can effectively reduce the flux leakage without a significant decline of the coupling coefficient. In the experiments, the designed WEVC system achieves an output of 6.6 kW at the maximum transmission efficiency of 95%. The experimental results show that the proposed structure not only performs well in terms of the misalignment tolerance but also enables the EMF emissions less than 27 $\mu\mathrm{T}_{\mathrm{RMS}}$.

References

[1] C. C. Mi, G. Buja, S. Y. Choi, and C. T. Rim, "Modern advances in wireless power transfer systems for roadway powered electric vehicles," *IEEE Trans. Ind. Electron.*, vol. 63, no. 10, pp. 6533–6545, Oct. 2016.

[2] S. Hui, W. Zhong, and C. Lee, "A critical review of recent progress in mid-range wireless power transfer," *IEEE Trans. Power Electron.*, vol. 29, no. 9, pp. 4500–4511, Sep. 2014.

[3] H. Zeng, Z. Liu, Y. Hou, T. Hei, and B. Zhou, "Optimization of magnetic core structure for wireless charging coupler," *IEEE Trans. Magn.*, vol. 53, no. 6, Jun. 2017, Art no. 8000804.

[4] G. Yang *et al.*, "Interoperability improvement for wireless electric vehicle charging system using adaptive phase-control transmitter," *IEEE Access*, vol. 7, pp. 41365–41379, 2019.

[5] L. Zhao, D. J. Thrimawithana, U. K. Madawala, A. P. Hu, and C. C. Mi, "A misalignment tolerant series-hybrid wireless EV charging system with integrated magnetics," *IEEE Trans. Power Electron.*, vol. 34, no. 2, pp. 1276–1285, Feb. 2019.

[6] O. C. Onar, J. M. Miller, S. L. Campbell, C. Coomer, C. P. White, and L. E. Seiber, "Oak ridge national laboratory wireless power transfer development for sustainable campus initiative," in *Proc. IEEE Transp. Electrific. Conf. Expo.*, Jun. 2013, pp. 1–8.

[7] Z. Li, K. Song, J. Jiang, and C. Zhu, "Constant current charging and maximum efficiency tracking control scheme for supercapacitor wireless charging," *IEEE Trans. Power Electron.*, vol. 33, no. 10, pp. 9088–9100, Oct. 2018.

[8] Y. Chen, R. Mai, Y. Zhang, M. Li, and Z. He, "Improving misalignment tolerance for IPT system using a third-coil," *IEEE Trans. Power Electron.*, vol. 34, no. 4, pp. 3009–3013, Apr. 2019.

[9] M. Budhia, J. T. Boys, G. A. Covic, and C. Huang, "Development of a single-sided flux magnetic coupler for electric vehicle IPT charging systems," *IEEE Trans. Ind. Electron.*, vol. 60, no. 1, pp. 318–328, Jan. 2013.
[10] M. Budhia, G. A. Covic, J. T. Boys, and C. Y. Huang, "Development and evaluation of single sided flux couplers for contactless electric vehicle charging," in *Proc. IEEE Energy Convers. Congr. Expo.*, Sep. 2011, pp. 614–621.
[11] A. Zaheer, H. Hao, G. A. Covic, and D. Kacprzak, "Investigation of multiple decoupled coil primary pad topologies in lumped IPT systems for interoperable electric vehicle charging," *IEEE Trans. Power Electron.*, vol. 30, no. 4, pp. 1937–1955, Apr. 2015.
[12] SAE J2954. Task Force on Wireless Power Charging. April, 2019. [Online]. Available: http://www.sae.org
[13] W. Li, J. Lu, G. Zhu, W. Zhang, and J. Jiang, "Design and research of a double-sided flux coupler in inductive power transfer system," in *Proc. 42th Annu. IEEE Ind. Electron. Soc. Conf.*, Oct. 2016, pp. 6033–6037.
[14] Y. Li, J. Zhao, Q. Yang, L. Liu, J. Ma, and X. Zhang, "A novel coil with high misalignment tolerance for wireless power transfer," *IEEE Trans. Magn.*, vol. 55, no. 6, pp. 1–4, Jun. 2019
[15] E. P. Li *et al.*, "Progress review of electromagnetic compatibility analysis technologies for packages, printed circuit boards, and novel interconnects," *IEEE Trans. Electromagn. Compat.*, vol. 52, no. 2, pp. 248–265, May 2010.
[16] M. Mohammad *et al.*, "Design of an EMF suppressing magnetic shield for a 100-kW DD-Coil wireless charging system for electric vehicles," in *Proc. IEEE Appl. Power Electron. Conf. Expo.*, 2019, pp. 1521–1527.
[17] F. Y. Lin, A. Zaheer, M. Budhia, and G. A. Covic, "Reducing leakage flux in IPT systems by modifying pad ferrite structures," in *Proc. IEEE Energy Convers. Congr. Expo.*, Sep. 2014, pp. 1770–1777.
[18] S. Y. Choi, J. Huh, W. Y. Lee, and C. T. Rim, "Asymmetric coil sets for wireless stationary EV chargers with large lateral tolerance by dominant field analysis," *IEEE Trans. Power Electron.*, vol. 29, no. 12, pp. 6406–6420, Dec. 2014.
[19] F. Y. Lin, S. Kim, G. Covic, and J. T. Boys, "Effective coupling factors for series and parallel tuned secondaries in IPT systems using bi-polar primary pads," *IEEE Trans. Transp. Electrific.*, vol. 3, no. 2, pp. 434–444, Jun. 2017.
[20] J. Kim *et al.*, "Coil design and shielding methods for a magnetic resonant wireless power transfer system," *Proc. IEEE*, vol. 101, no. 6, pp. 1332–1342, Jun. 2013.
[21] F. Y. Lin, G. A. Covic, and J. T. Boys, "Evaluation of magnetic pad sizes and topologies for electric vehicle charging," *IEEE Trans. Power Electron.*, vol. 30, no. 11, pp. 6391–6407, Nov. 2015.

Kai Song (Senior Member, IEEE) received the B.S. and Ph.D. degree in electrical engineering and automation from the Harbin Institute of Technology (HIT), Harbin, China, in 2005 and 2011, respectively.

In 2011, He joined the School of Electrical Engineering and Automation, HIT, as a Lecturer. He was a Visiting Scholar in electrical engineering with The University of Tokyo, Japan, from 2014 to 2015. He is currently an Associate Professor with HIT, where he has been the Deputy Director of the Institute of Wireless Power Transfer Technology, since 2016. He has coauthored more than 60 peer-reviewed technical papers and authorized 30 invention patents in China. His current research interests include wireless power transfer, particularly in wireless charging systems for electric vehicles.

Guang Yang received the B.S. degree in instrumentation science and technology from the School of Electrical and Information Engineering, Anhui University of Technology (AHUT), Ma'anshan, China, in 2014, and the M.S. degree in instrumentation science and technology in 2017 from the School of Electrical Engineering and Automation, Harbin Institute of Technology (HIT), Harbin, China, where he is currently working toward the Ph.D. degree in electrical engineering.

His research interests include wireless charging technology for electric vehicles and other applications.

Mr. Yang was the recipient of the Best Paper Award from the 22nd International Conference on Electrical Machines and Systems.

Yu Guo received the B.S. and M.S. degrees in instrumentation science and technology from the School of Electrical Engineering and Automation, Harbin Institute of Technology, Harbin, China, in 2017 and 2019, respectively.

She is currently an Engineer with Shenzhen Inovance Technology Company, Ltd., Shenzhen, China. Her research interests include wireless power transfer and on-board charging applications.

Yu Lan is currently working toward the B.S. degree with the School of Instrumentation Science and Engineering, Harbin Institute of Technology, Harbin, China.

His research interest concentrates in wireless power transfer for electric vehicle applications.

Shuai Dong received the M.S. and Ph.D. degrees in electrical engineering from the Harbin Institute of Technology (HIT), Harbin, China, in 2011 and 2016, respectively.

He has been a Lecturer with the School of Electrical Engineering & Automation, HIT, since 2017. He specializes in the research field of wireless power transfer and power electronics for electric vehicle applications.

Jinhai Jiang received the B.S. and M.S. degrees from School of Electrical Engineering & Information, Northeast Petroleum University, Daqing, China, in 2010 and 2013, respectively, and the Ph.D. degree in electrical engineering from the Harbin Institute of Technology (HIT), Harbin, China, in 2019.

He is currently a Lecturer with the School of Electrical Engineering & Automation, HIT. His research interests include wireless power transfer for super capacitor and battery-powered online electric vehicles.

Chunbo Zhu (Member, IEEE) received the B.S. and M.S. degrees in electrical engineering and the Ph.D. degree in mechanical engineering from the Harbin Institute of Technology (HIT), Harbin, China, in 1987, 1992, and 2001, respectively.

He was a Postdoctoral Research Fellow with the PEI Research Center, National University of Ireland, Galway, Ireland, from 2003 to 2004. He has been a Lecturer with the Department of Automation Measurement and Control, HIT, since 1987. He is currently a Full Professor with HIT, where he leads the Laboratory of Wireless Power Transfer and Battery Management Technologies. His current research interests include energy management systems, electric and hybrid electric vehicles, and wireless power transfer technologies.